ELSEVIER

Chemical Engineering Journal 133 (2007) 173–186

Chemical Engineering Journal

www.elsevier.com/locate/cej

Pressure and flow distribution in pipe and ring spargers: Experimental measurements and CFD simulation

A.V. Kulkarni [1], Swarnendu S. Roy, J.B. Joshi *

Institute of Chemical Technology, University of Mumbai, Matunga, Mumbai 400 019, India

Received 13 November 2006; received in revised form 21 February 2007; accepted 1 March 2007

Abstract

In case of low H_D/D ratio bubble columns, the sparger design dominates the performance of the bubble column reactor. However, scanty information is available in the published literature regarding the flow distribution in sparger. In view of this a comprehensive study was undertaken for a single pipe sparger and ring sparger covering a wide range of hole diameters (2–6 mm), pitch (2–8d_o), pipe length (0.6 m and 1.5 m), ring diameter (0.38–0.57 m) and pipe diameter of rings (0.012–0.019 m). The flow variations have been related to geometric and operating parameters. Theoretical models available in the literature for pipe sparger have been critically analyzed. CFD simulations (ANSYS CFX-10) have been performed for all the pipe spargers and the results have been compared with the model of Acrivos et al. [A. Acrivos, B.D. Babcock, R.L. Pigford, Flow distributions in manifolds, Chem. Eng. Sci. 10 (1959) 112–124]. CFD simulations of all the ring spargers also have been performed, and the predictions show favorable agreement with experimental values of pressure and hole velocity.

Keywords: Pipe sparger; Ring sparger; CFD; Flow distribution; Manifold; Bubble column

1. Introduction

Uniformity in sparging of lighter phase into the heavier phase in multiphase reactors is one of the key parameters which mostly dictate the performance of reactors. Uniformity results into high values of interfacial area and mass transfer coefficient. Further, it gives rise to lower level of liquid phase back mixing and reduces the possibility of dead zones. On the other hand, non-uniformity results into higher pressure drop and introduces the possibility of clogging some holes. Hence, the design of proper sparger is one of the most important aspects of process design of multiphase reactors, such as bubble column. Various types of spargers are in commercial use, which can be broadly classified as plate type and pipe type. In plate type spargers, sieve plate design is widely used. In the category of pipe type, commonly employed designs are ring type (single and multiple rings) spargers, spiders, pipe spargers, etc. The plate type spargers are suitable for relatively small diameter columns and the pipe type spargers are used for large diameter columns. The typical spargers used commercially are shown in Fig. 1.

The objective of uniform sparging in pipe type sparger can be achieved if the pressure of fluid in the pipe remains constant along the length. The pressure in pipe varies along the length in two ways, as: (1) pressure falls in the direction of flow due to friction with the internal surface of the pipe, whereas, (2) pressure rise occurs in the direction of flow due to reduction of fluid momentum owing to the deceleration of the fluid along the length as it continuously escapes from the holes. Therefore, to obtain uniform pressure along the pipe, it is necessary to have a proper balance between the pressure rise due to flow branching and the pressure drop due to friction. However, the flow inside this simple type of sparger is fairly complex, and it depends strongly on the geometrical parameters such as pipe and hole diameter, pipe length, pitch, etc. Therefore, it is very useful to predict the flow distribution inside the sparger for its efficient design. Several theoretical models are available in the published literature for the prediction of flow distribution inside the pipe sparger. A brief account of these models has been given in the next section. Alternatively, CFD can be a useful tool for the prediction of flow pattern inside the spargers and no effort has been reported in this direction.

* Corresponding author. Tel.: +91 22 414 5616; fax: +91 22 414 5614.
E-mail address: jbj@udct.org (J.B. Joshi).
[1] Present address: Larsen & Toubro Ltd., EPC Centre, Ashish Complex, NH 8, Chhani, Vadodara 391740, India.

1385-8947/$ – see front matter © 2007 Elsevier B.V. All rights reserved.
doi:10.1016/j.cej.2007.03.011

Nomenclature

A_o	cross-sectional area of hole (m^2)
A_p	cross-sectional area of pipe sparger (m^2)
a	free area per unit length of pipe (m^2/m)
C	orifice discharge coefficient
C_μ	constant in k–ε model
$C_{\varepsilon 1}$	model parameter in turbulent dissipation energy equation
$C_{\varepsilon 2}$	model parameter in turbulent dissipation energy equation
d_o	hole diameter (m)
D	bubble column diameter (m)
D_p	diameter of pipe (m)
E	length to diameter ratio of pipe sparger (L_e/D_p)
ENU	extent of non-uniformity (%)
Eu	Euler number ($2(P_{in} - P_{out})/\rho V_{in}^2$)
Eu_x	Euler number ($2\Delta P/\rho V_{in}^2$)
f	fanning friction factor
f_{av}	average fanning friction factor
f'	friction factor for smooth pipe
F_0	constant defined in Eq. (5)
FA	free area based on surface area of a single pipe
g	gravitational constant (m/s^2)
G	generation term (W/m^3)
H_D	height of dispersion (m)
k	turbulent kinetic energy per unit mass (m^2/s^2)
k'	momentum recovery factor
L	length of pipe (m)
L_e	effective length of pipe (m)
n	number of holes
P	pressure (Pa)
ΔP	pressure change along the pipe (Pa)
ΔP_i	pressure change between ith and $(i+1)$th hole in the pipe (Pa)
P_i'	pressure just upstream of ith hole (Pa)
P_i^0	pressure just downstream of ith hole (Pa)
P_{in}	pressure at the start of sparger holes (Pa)
ΔP_L	pressure drop across the last hole from the entrance (Pa)
ΔP_o	pressure change across hole (Pa)
ΔP_{o1}	pressure drop across the first hole from the entrance (Pa)
P_{out}	pressure outside the sparger (Pa)
q	constant defined by Eq. (12)
r	constant defined by Eq. (12)
Re	Reynolds number
Re_0	Reynolds number at the inlet
s	constant defined by Eq. (12)
t	time (s)
$\mathbf{u}$	velocity vector (m/s)
U	dimensionless velocity in the pipe (V_p/V_{in})
V_o	hole velocity (m/s)
V_i'	velocity just upstream of ith hole (m/s)
V_i^0	velocity just downstream of ith hole (m/s)
V_{in}	velocity at the inlet of pipe (m/s)
V_p	velocity in pipe (m/s)
W_{in}	mass flow rate at the inlet of pipe (kg/s)
W_o	mass discharge flow rate through orifices per unit length (kg/s m)
x	distance to location along the main header under consideration (m)
$\bar{x}$	dimensionless distance along the pipe (x/L)
Δx	pitch (m)
y	constant defined in Eq. (5)

Greek symbols

α	constant in Eq. (26)
α_0	fraction of internal area of tube occupied by discharge port
β	constant in Eq. (26)
ε	turbulent energy dissipation rate per unit mass (m^2/s^3)
μ	fluid viscosity (Pa s)
μ_{eff}	effective fluid viscosity (Pa s)
μ_T	turbulent viscosity (Pa s)
ξ	constant in Eq. (26)
ρ	fluid density (kg/m^3)
σ_k	Prandtl number for turbulent kinetic energy
σ_ε	Prandtl number for turbulent energy dissipation rate
τ	shear stress (Pa)

In the present paper, a systematic investigation of single pipe and single ring spargers has been presented. Experiments have been performed to measure the pressure drop characteristics and the uniformity of gas distribution covering a wide range of hole diameters (2–6 mm), pitch (2–8d_o), pipe length (0.6 m and 1.5 m), ring diameter (0.38–0.57 m) and pipe diameter of rings (0.012–0.019 m). A systematic analysis of the available theoretical models has been undertaken with respect to the experimental data. Further, CFD simulations were also carried out to predict the pressure and flow distribution in pipe and ring spargers. A critical analysis of the available theoretical models has been presented and the relative merit of CFD simulation has been brought out.

2. Literature review

The flow distribution through the sparger holes depends upon the inlet gas energy (pressure and kinetic), frictional losses along the pipe and the geometry of holes (size, number, location, orientation, etc.). Senecal [1] have performed systematic experiments for achieving uniformity of distribution within 95%. On the basis of large number of observations, they have proposed the following empirical criteria in terms of permissible ratios of (a) the kinetic energy per unit mass at the inlet to the pressure drop across the sparger hole and (b) the pressure drop (frictional)

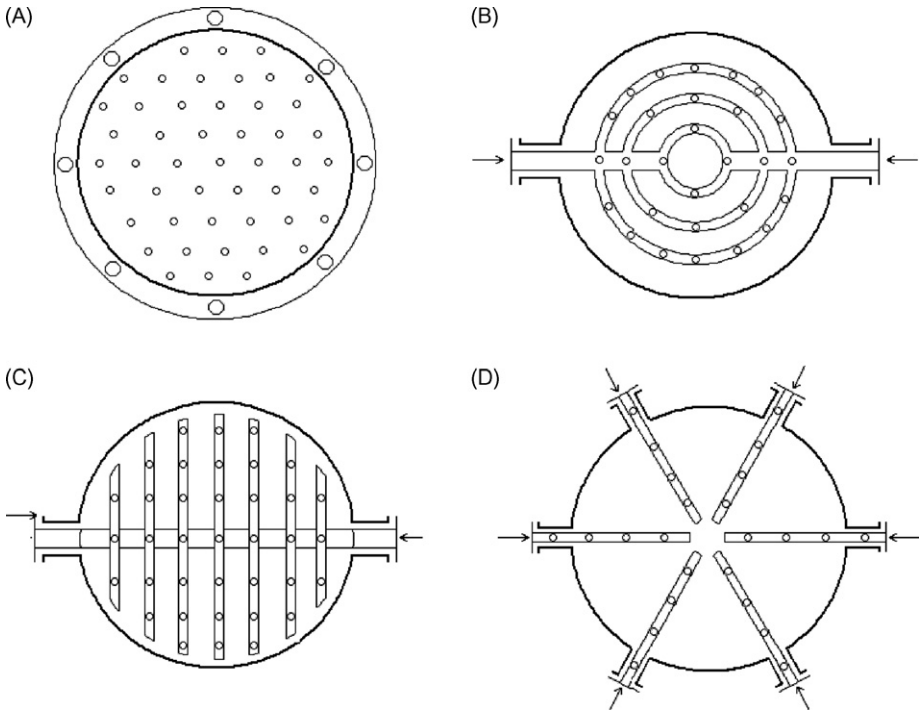

Fig. 1. Spargers for bubble column reactor: (A) sieve plate sparger; (B) multiple ring sparger; (C) spider; (D) pipe sparger.

along the pipe to that across the hole:

$$\frac{\rho V_{\text{in}}^2/2}{\Delta P_{\text{o}}} \leq 0.1 \tag{1}$$

and

$$\frac{\Delta P}{\Delta P_{\text{o}}} \leq 0.1 \tag{2}$$

The author has also given an equation for estimation of percent maldistribution between the first and the last hole and is given by

$$\text{maldistribution}\,(\%) = 100\left(\sqrt{\frac{\Delta P_{\text{o1}} - \Delta P_{\text{L}}}{\Delta P_{\text{o1}}}} - 1\right) \tag{3}$$

where ΔP_{o1} and ΔP_{L} are the values of pressure drop at the first hole and the last hole of the pipe, respectively. Accordingly, when the friction is dominant (very long pipe or small diameter pipe or very low velocity at the inlet), the holes near the entrance discharge more in comparison with the later holes. On contrary, if the kinetic energy at the inlet is much higher than the frictional pressure drop along the pipe (i.e. short pipe or large diameter) the holes at the rear end discharge more than the entrance holes. Though Eqs. (1)–(3), give the estimate of maldistribution, they do not provide clear recommendations for the demarcation between 'friction dominant' and 'kinetic energy dominant' conditions, in terms of inlet velocity, pipe diameter or the ratio of hole diameter to pipe diameter. Further, no procedure has been suggested for the selection of hole diameter, pitch, number of holes and their orientation.

Acrivos et al. [2] have performed an extensive experimental and theoretical study to obtain pressure and flow distribution in the straight pipe sparger. They established momentum balance along the pipe by including frictional pressure drop and the pressure rise due to continuous reduction in the kinetic head because of the orifice discharge as follows

$$\left(\frac{\mathrm{d}^2U}{\mathrm{d}y^2}\right)\left(\frac{\mathrm{d}U}{\mathrm{d}y}\right) + U\left(\frac{\mathrm{d}U}{\mathrm{d}y}\right) + F_0U^{7/4} = 0 \tag{4}$$

where

$$F_0 \equiv \frac{f}{2^{5/2}k'^{3/2}\alpha_0 C}, \qquad y \equiv \left(\frac{4\alpha_0 C}{D_{\text{P}}}\sqrt{2k'}\right)x \tag{5}$$

Thus, the flow through each hole depends upon the local pressure driving force. The differential momentum balance (Eq. (4)) was solved for a given set of known inlet pressure, inlet velocity, hole diameter, pitch and friction factor. They had considered the variation of F_0 as a function of velocity along the length of the pipe. The proposed model is in the most generalized form among the models available in the literature. Still it suffers from disadvantage in terms of choosing the values of momentum recovery factor (k'), orifice coefficient (C) and friction factor (f). For their experimental cases they had proposed values of k', C which predict experimental data, however, they do not hold for other cases as the model parameters are strongly dependent on the flow rate as well as the geometry under consideration.

Cooper [3] has provided another approach to the problem. He derived an expression for the pressure profile along the pipe, which is then utilized to evaluate the relationship between the free area and the pipe length as given by

$$a = f(x) \tag{6}$$

If W_o is the mass discharge flow rate through orifices per unit length of the pipe (kg/m s), the orifice equation gives the following relationship:

$$W_o\,dx = C\rho\sqrt{\frac{2(P-P_{out})}{\rho}}f(x)\,dx \tag{7}$$

Substitution of Eq. (6) in Eq. (7) gives

$$f(x) = \frac{W_o}{C\sqrt{2\rho(P-P_{out})}} \tag{8}$$

The Fanning friction factor equation in the differential form is given by

$$\frac{dP}{dx} = -\frac{4f}{D_p}\frac{\rho V_P^2}{2} \tag{9}$$

The mass flow rate (W, kg/s) decreases along the length and at any location (x) the value of W is given by

$$W = W_{in} - W_o x \tag{10}$$

The local Reynolds number in terms of mass flow rate is given by

$$Re = \frac{4(W_{in}-W_o x)}{\pi D_P \mu} \tag{11}$$

The author selected the following constants:

$$q = \frac{2}{A_p^2 D_p}, \quad r = \frac{4}{\pi D_p \mu}, \quad s = r^{-0.42} \tag{12}$$

where A_p is the pipe cross-sectional area, D_p the pipe diameter, C the orifice discharge coefficient and μ is the viscosity. Substituting, these constants in Eq. (9) and by selecting the following equation for friction factor:

$$f = 0.0035 + 0.264Re^{-0.42} \tag{13}$$

Eq. (10), takes the following form:

$$-\frac{dP}{dx} = [0.0035q(W_{in}-W_o x)^2 + 0.264qs(W_{in}-W_o x)^{1.58}]\frac{dx}{\rho} \tag{14}$$

Eq. (14) was integrated for the case of low values of pressure drop along the pipe. The escape area (a) along the pipe was further evaluated by inserting the integral of Eq. (14) in Eq. (8). The resulting pressure profile along the pipe thus obtained is as follows

$$P = P_{in} - \left(\frac{0.00117q}{W_o\rho}\right)[W_{in}^3 - (W_{in}-W_o x)^3] - \left(\frac{0.102qs}{W_o\rho}\right)[W_{in}^{2.58} - (W_{in}-W_o x)^{2.58}] \tag{15}$$

The uniform flow was obtained by varying the pitch of the hole from a maximum at the beginning to a minimum at the dead end. The biggest limitation of this model is that it takes only Fanning's equation as the basis, which does not consider the phenomena of pressure change due to the change of momentum. Hence, the pressure calculated from this equation shows only a fall from the entrance to the dead end, as expected from Fanning's equation. Although, this technique of variation of free area along the pipe length is useful to obtain uniform distribution, it may be pointed out that the sparger design for one flow rate may not give uniform distribution for any other flow rate.

Greskovich and O'Bara [4] have calculated the pressure distribution using summation technique rather than the integral approach as in the case of the model of Acrivos et al. [2]. They have assumed the same velocity through all the holes and obtained the following equation for the pressure variation:

$$\left(\frac{\Delta P}{\rho}\right)_{total} = \frac{2f_{av}LV_{in}^2}{D_p}\left\{\sum_{i=1}^{n}\frac{[n-(i-1)/n]^2}{n}\right\} - k'\left[1-\frac{1}{n^2}\right]V_{in}^2 \tag{16}$$

where the pipe length has been divided into n sections according to the number of orifices and i denotes the ith section. For large values of n, i.e. large number of holes, the summation in the first term reduces to an asymptotic value of 0.33 (typically for $n > 12$). Hence, Eq. (16) reduces to the following form:

$$\left(\frac{\Delta P}{\rho}\right)_{total} = 0.66\frac{2f_{av}LV_{in}^2}{D_p} - k'V_{in}^2 \tag{17}$$

Thus, this model is a simplified version of the model proposed by Acrivos et al. [2], and does not offer any advantages over the former model. Further, the assumption of the uniform flow through each hole is a major limitation in using this model.

Knaebel [5] extended the work of Senecal [1] for pipe spargers and has recommended critical hole diameter for 95% uniformity of gas distribution. For this purpose, he substituted orifice equation in Eq. (1) and obtained the following expression:

$$d_o \le \frac{0.7D_p}{(0.27+n^2)^{0.25}} \tag{18}$$

Since, n, number of holes is usually large, the above equation reduces to

$$d_o \le \frac{0.7D_p}{\sqrt{n}} \tag{19}$$

Alternatively Knaebel [5] obtained another expression by substituting orifice and Fanning friction factor equations in Eq. (2). Further, he assumed that the frictional loss in the pipe is approximately one velocity head per 150 pipe diameters. Under this set of assumptions, the critical d_o was given by the following equation:

$$d_o = \frac{D_p}{(1+n^2L/41.66D_p)^{0.25}} \tag{20}$$

Constraint on the hole diameter provided by Eq. (20) is particularly useful, when L/D_p ratio is higher than 150. When it is less than 150, the author has recommended Eq. (18). In this work, the assumption of friction loss of one velocity head per 150 pipe diameter is prohibitive since the friction loss for pipe

distributors varies over a wide range and usually not known *a priory*. Further, the use of Fanning equation for entire length of the pipe is also questionable as this equation cannot take pressure rise into account.

Wang et al. [6] used the same set of basic equations for the case of porous pipe sparger. They allowed the values of k' to vary along the pipe according to the local pipe velocity. But unlike Acrivos et al. [2] they have not considered the variation of f along the pipe which is a major limitation of their model. They assumed uniform flow through the holes which also means linear variation of the flow within the sparger with a maximum at the inlet to zero at the dead end. The following equations were obtained for the momentum balance, mass balance and the orifice discharge, respectively:

$$\frac{1}{\rho}\frac{\mathrm{d}P}{\mathrm{d}x} - \frac{f}{2D_\mathrm{p}}V_\mathrm{p}^2 + 2V_\mathrm{p}\frac{\mathrm{d}V_\mathrm{p}}{\mathrm{d}x} + \frac{A_\mathrm{o}n}{A_\mathrm{p}L}V_\mathrm{o}V_\mathrm{p} = 0 \tag{21}$$

$$V_\mathrm{o} = -\frac{A_\mathrm{p}L}{A_\mathrm{o}n}\frac{\mathrm{d}V_\mathrm{p}}{\mathrm{d}x} \tag{22}$$

$$P - P_\mathrm{out} = C\rho\frac{V_\mathrm{o}^2}{2} \tag{23}$$

The velocity of fluid after discharge ($V_{\mathrm{p}\,i+1}$) was then expressed in terms of the velocity of fluid before discharge ($V_{\mathrm{p}\,i}$):

$$V_{\mathrm{p}\,i+1} = (2 - 2k')V_{\mathrm{p}\,i} \tag{24}$$

Substituting Eqs. (24) and (22) in Eq. (21), the differential momentum balance becomes

$$\frac{1}{\rho}\frac{\mathrm{d}P}{\mathrm{d}x} - \frac{f}{2D_\mathrm{p}}V_\mathrm{p}^2 + 2k'V_\mathrm{p}\frac{\mathrm{d}V_\mathrm{p}}{\mathrm{d}x} = 0 \tag{25}$$

The friction factor and momentum recovery factor were assumed to have the following relationships:

$$f = \xi f' \quad \text{and} \quad k' = \alpha + \beta\frac{\Delta V_{\mathrm{p}(i,i+1)}^2}{V_{\mathrm{p}\,i}^2} \tag{26}$$

where f' is the friction factor for smooth pipe, which is a function of Reynolds number. α is the pressure recovery factor through the first hole. α and β both depend upon the geometry of the pipe sparger. The momentum recovery factor was further simplified based on the assumption of linear drop in the flow rate along the pipe, and hence the following equation was obtained

$$k' = \alpha + 2\beta\left(1 - \frac{x}{L}\right) \tag{27}$$

Inserting friction factor variation from Eq. (26) and momentum recovery factor variation from Eq. (27) into Eq. (25), the following relationship was obtained

$$\frac{1}{\rho}\frac{\mathrm{d}p}{\mathrm{d}x} + \frac{\xi f(Re)}{2D_\mathrm{p}}V_\mathrm{o}^2\left(1 - \frac{x}{L}\right)^2 + V_\mathrm{o}^2\left[\alpha + 2\beta\ln\left(1 - \frac{x}{L}\right)\right]\frac{\mathrm{d}(1 - x/L)^2}{\mathrm{d}x} = 0 \tag{28}$$

The friction factor (f') variation for a smooth pipe was selected depending on the flow regime, i.e. laminar, transition or turbulent and in the form of $f(Re_0)$. The solution for turbulent flow was obtained for the case of $\xi = 1$ and f' given by the following equation:

$$f' = \frac{0.3164}{Re^{0.25}} \quad \text{for} \quad 2200 < Re < 10^5 \tag{29}$$

Substitution of Eq. (29) in Eq. (28) and subsequent integration gives

$$Eu_x = \alpha[1 - (1 - \bar{x})^2] - \frac{0.058E}{Re_0^{0.25}}[1 - (1 - \bar{x})^{2.75}] - 2\beta[(1 - \bar{x})^2\ln(1 - \bar{x}) - 0.5\bar{x}(\bar{x} - 2)] \tag{30}$$

The authors have shown a good agreement between the experimental and the predicted pressure variation along the pipe distributor. However, the assumption of uniform flow through all the holes seems to be restrictive. Authors have not provided experimental support for the variation of k' along the pipe. Also, no methodology has been provided to achieve uniform flow distribution.

From the foregoing discussion, it can be seen that, though the modeling of straight pipe sparger has received fairly good attention, practically no information is available for ring sparger. Furthermore, the experimental data are also scarce, which cover a wide range of hole diameter, pitch, number of holes, and the length of pipe. The suggested methods to achieve the uniform sparging also have restricted applicability, because it either involves variation of cross-sectional area along the pipe [2] or variation of free area (hole area) along the pipe [3]. It is difficult to fabricate a pipe sparger with a variable cross-section or free area. Further, a pipe designed for a particular inlet velocity may not deliver uniform flow at any other velocity. One major limitation of the available models is the choice of proper values of all the parameters such as the orifice discharge coefficient, the momentum recovery coefficient and the friction factor. This limitation can be mitigated by the use of CFD tool. With proper boundary conditions CFD can predict both pressure and flow inside the sparger without the direct knowledge of k', C. These parameters can be taken into account in CFD by creation of a proper geometry and the grid. In view of this, it was thought desirable to undertake a systematic experimental investigation over a wide range of hole diameter, pitch, number of holes and pipe length and to validate the CFD model with the experimental data. The CFD model thus developed can be used to design the pipe and ring spargers.

3. Experiments

Experiments were performed with 10 straight pipe distributors and 5 perforated rings. In pipe sparger, hole diameter was varied from 2 mm to 5 mm, pitch in the range of 2–8d_o, and the total length of 0.6 m and 1.5 m. In case of rings, hole diameter was varied from 2.5 mm to 6 mm. The geometrical details in terms of hole diameter, pitch, number of holes and active length,

Table 1A
Geometric details of pipe spargers

Pipe sparger	Pipe diameter, ID (mm)	d_o (mm)	Pitch	No. of holes	Free area of holes cross/sectional area of pipe
P1	28	2	$2d_o$	110	0.561
P2	28	2	$8d_o$	28	0.143
P3	28	3	$2d_o$	71	0.815
P4	28	3	$4d_o$	35	0.401
P5	28	3	$8d_o$	18	0.207
P6	28	5	$8d_o$	14	0.446
P7	28	2	$4d_o$	185	0.944
P8	28	2	$8d_o$	93	0.474
P9	28	5	$4d_o$	69	2.200
P10	28	5	$8d_o$	35	1.116

Table 1B
Geometric details of ring sparger

Ring sparger	Pipe diameter (m)	Ring diameter (m)	d_o (mm)	Pitch (m)	No. of holes	Free area of holes cross-sectional area of pipe
R1	0.012	0.4	2.5	0.055	23	0.998
R2	0.012	0.4	4	0.055	23	2.555
R3	0.012	0.4	6	0.055	23	5.75
R4	0.019	0.38	6	0.057	21	2.094
R5	0.019	0.57	6	0.085	21	2.094

Table 2A
Location of pressure taps for small pipe

Location	Distances (m)		
	P1 and P2	P3–P5	P6
Entrance	0	0	0
Pr1	0.21	0.21	0.30
Pr2	0.39	0.39	0.48
Pr3	0.56	0.56	0.65

Table 2C
Location of pressure taps for ring

Location	Linear distances, $(d_r/2)\theta$ (m)		
	R1–R3	R4	R5
Pr1	0.10	0.05	0.06
Pr2	0.47	0.45	0.68
Pr3	0.77	0.74	1.12
Pr4	1.16	1.15	1.73

i.e. length of the pipe from first hole to last hole, etc., are given in Table 1A and that for rings in Table 1B, respectively. The ambient air was used for all the experiments. Volumetric flow rate was measured by using precalibrated rotameter. The pressure along the pipe was measured at four and six locations for the pipe lengths of 0.6 m and 1.5 m, respectively, using water barometer and the details of pressure tap locations are given in Tables 2A and 2B. In case of rings the pressure was measured at four locations on the ring (details are given in Table 2C) and one at the entrance. The measurement accuracy was ±10 Pa. All the experiments were performed twice and the average was used for calculations. The reproducibility in the measurements was of the order of accuracy of the measurement variable.

Table 2B
Location of pressure taps for long pipe

Location	Distances (m)	
	P7 and P8	P9 and P10
Entrance	0	0
Pr1	0.40	0.50
Pr2	0.70	0.75
Pr3	1.00	1.06
Pr4	1.30	1.37
Pr5	1.60	1.71

4. Computational model

4.1. Governing equations

The equations of continuity, motion, turbulent kinetic energy (k) and turbulent energy dissipation rate (ε) for three-dimensional cylindrical co-ordinate system for single phase flow can be represented by the following governing equation:

$$\frac{\partial \rho}{\partial t} + \nabla \cdot (\rho \mathbf{u}) = 0 \tag{31}$$

$$\frac{\partial}{\partial t}(\rho \mathbf{u}) + \nabla \cdot (\rho \mathbf{u}\mathbf{u}) = -\nabla \cdot \tau - \nabla P + \rho g \tag{32}$$

where P is the static pressure, τ the stress tensor and ρg is the gravitational body force. The stress tensor is given by

$$\tau = -\mu_{\text{eff}}(\nabla \mathbf{u} + (\nabla \mathbf{u})^{\text{T}} - \tfrac{2}{3} I(\nabla \cdot \mathbf{u})) \tag{33}$$

where

$$\mu_{\text{eff}} = \mu + \mu_{\text{T}} \tag{34}$$

The turbulent eddy viscosity is formulated as follows

$$\mu_{\mathrm{T}} = \rho C_{\mu} \frac{k^2}{\varepsilon} \tag{35}$$

The turbulent kinetic energy k and dissipation rate ε are calculated from their governing equations:

$$\frac{\partial}{\partial t}(\rho k) + \nabla \cdot (\rho \mathbf{u} k) = \nabla \cdot \left(\frac{\mu_{\mathrm{eff}}}{\sigma_k} \nabla k \right) + (G - \rho\varepsilon) \tag{36}$$

$$\frac{\partial}{\partial t}(\rho \varepsilon) + \nabla \cdot (\rho \mathbf{u} \varepsilon) = \nabla \cdot \left(\frac{\mu_{\mathrm{eff}}}{\sigma_{\varepsilon}} \nabla \varepsilon \right) + \frac{\varepsilon}{k}(C_{\varepsilon 1} G - C_{\varepsilon 2} \rho \varepsilon) \tag{37}$$

The model constants are $C_{\mu} = 0.09$; $\sigma_k = 1.00$; $\sigma_{\varepsilon} = 1.3$ $C_{\varepsilon 1} = 1.44$, $C_{\varepsilon 2} = 1.92$. The term G in above equation is the production of turbulent kinetic energy and described by

$$G = \tau : \nabla \mathbf{u} \tag{38}$$

4.2. Numerical details

Three-dimensional (3D) steady state numerical simulations were carried out for the geometry of Acrivos et al. [2] and for all the 10 pipes and 5 rings geometries stated in Tables 1A and 1B, respectively. ANSYS CFX-10 was used for all the simulations. ANSYS ICEM CFD-10 was used to generate tetra grid along with five layer of prism mesh for all the geometries. The number of grid were varied from 0.4 to 0.7 million depending on the hole size of the spargers and overall dimension. For all simulations, pressure was specified at the sparger inlet and the mass flow rate was specified at the sparger outlet. The high resolution discretization scheme was used for the convective terms.

5. Results and discussion

5.1. Experimental results

Experiments of pressure measurement for 10 straight pipe spargers and for 5 ring spargers were carried with different inlet air velocity (in the range of 13–39 m/s for pipe spargers and 7–96 m/s for ring spargers). For the estimation of hole velocity, the following orifice type of equation was considered

$$V_{\mathrm{o}} = C \sqrt{\frac{2}{\rho} \left(\frac{P_i' + P_i^0}{2} - P_{\mathrm{out}} \right)} \tag{39}$$

where P_{out} is the pressure at the outlet of the holes, C the orifice coefficient, and P_i' and P_i^0 are the values of pressure just upstream and just downstream of the ith hole. For the estimation of hole velocity, the measured discrete pressure values were fitted with a polynomial to get a continuous pressure profile along the pipe length. With the fitted pressure profile, Eq. (39) was solved to get the hole velocities with a constant value of C. The value of C was selected in such a way that the overall mass balance gets satisfied. The same procedure was followed for both

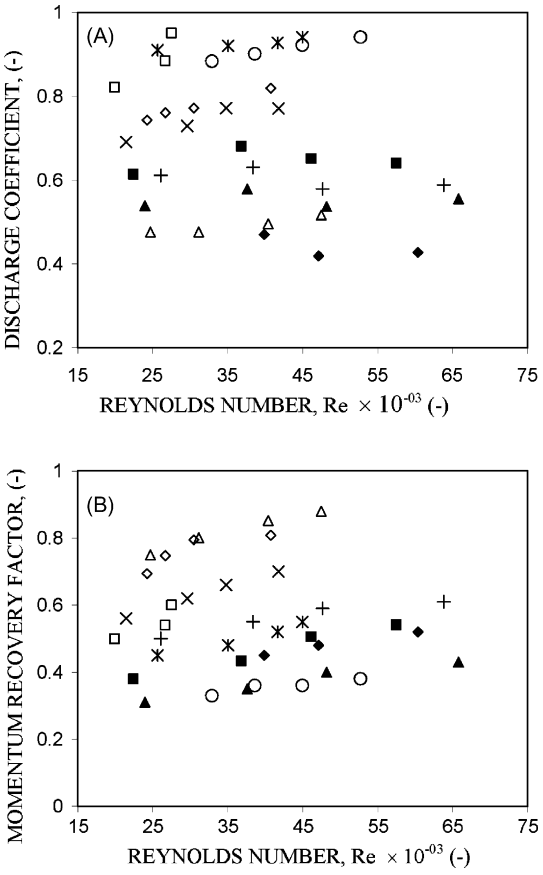

Fig. 2. Effect of Reynolds number and geometric parameters of sparger on: (A) orifice discharge coefficient; (B) momentum recovery factor. (◊) P1; (□) P2; (△) P3; (×) P4; (*) P5; (◯) P6; (+) P7; (■) P8; (♦) P9; (▲) P10.

the straight pipe and the ring spargers. Fig. 2A shows the variation of orifice discharge coefficient with Reynolds number for all the pipe spargers. The discharge coefficient increases with an increase in the Reynolds number for small pipe distributors, i.e. from P1 to P6. The Reynolds number dependence for short pipes is strong as compared with that for long pipe distributors, i.e. P7–P10. It can be seen that, for long pipes, the orifice discharge coefficient remains practically constant. For a particular hole diameter, discharge coefficient increases with an increase in the pitch for all the cases.

Since the kinetic head of the flow decreases because of every orifice discharge, it results into pressure recovery. The pressure recovery across a hole can be estimated as

$$P_i' - P_i^0 = k' \rho [(V_i^0)^2 - (V_i')^2] \tag{40}$$

where k' is the momentum recovery parameter, which takes into account all the non-idealities which do not permit complete conversion of velocity head into pressure head. V_i' and V_i^0 are the velocities just upstream and just downstream of the ith hole. The frictional pressure drop for the straight section between the two consecutive holes was estimated using the following Fanning equation:

$$\Delta P_i = -\frac{2\rho f V_i'^2 \Delta x}{D_{\mathrm{p}}} \tag{41}$$

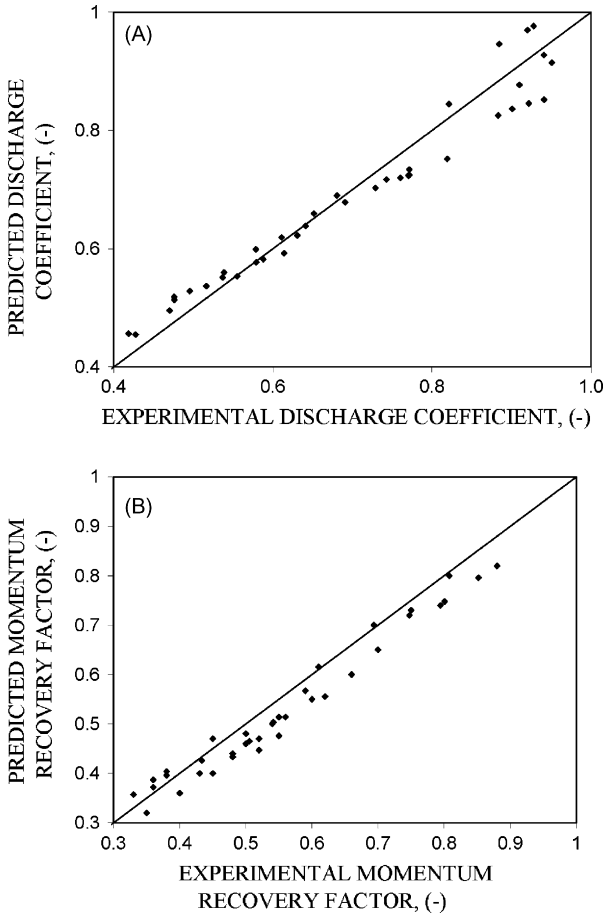

Fig. 3. Parity plot: (A) orifice discharge coefficient; (B) momentum recovery factor.

For the estimation of k', Eqs. (40) and (41) were used. For this purpose, known experimental pressure profile and the flow rate at each hole (obtained from Eq. (39)) were substituted in Eqs. (40) and (41) to obtain the values of k'. Fig. 2B shows the variation of momentum recovery factor with Reynolds number, for all the pipes. The momentum recovery factor increases with an increase in the Reynolds number and, for a particular hole diameter, an increase in the pitch results into a decrease in the pressure recovery factor.

It was thought desirable to develop correlations for C and k'. Following are the results with a correlation coefficient of 0.9, 0.9, respectively. The parity plots are shown in Fig. 3A and B, respectively.

$$C = 0.081 Re^{-0.016} Eu^{-0.328} \mathrm{FA}^{-1.64} \left(\frac{\Delta x}{d_o}\right)^{-1.63} \left(\frac{\Delta x}{L_e}\right)^{0.79} \quad (42)$$

$$k' = 0.03 Re^{0.30} Eu^{0.15} \left(\frac{\Delta x}{d_o}\right)^{-0.49} \mathrm{FA}^{0.012} \left(\frac{\Delta x}{L_e}\right)^{-0.05} \quad (43)$$

Due to pressure recovery phenomena, hole velocity also increases from start to end. For easy comparison the hole velocity values were normalized with respect to the velocity value at the first hole, as was done by Acrivos et al. [2]. This step is

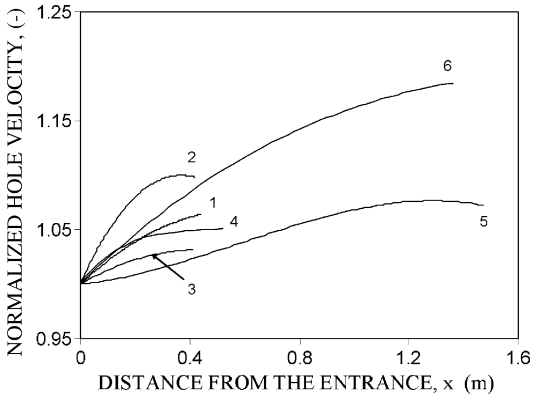

Fig. 4. Normalized hole velocity profile for straight pipe sparger: (1) P1 (V_{in} = 24.38 m/s); (2) P3 (V_{in} = 28.4 m/s); (3) P4 (V_{in} = 24.99 m/s); (4) P6 (V_{in} = 26.89 m/s); (5) P8 (V_{in} = 27.59 m/s); (6) P10 (V_{in} = 28.82 m/s).

useful to appreciate the extent of non-uniformity in the sparger. Figs. 4 and 5 show the normalized hole velocity for straight pipe (P1, P3, P4, P6, P8 and P10) and for all the rings, respectively. It can be seen that, for a straight pipe sparger (Fig. 4) the extent of non-uniformity increases with an increase in the hole diameter (P1–P3 and P8–P10), and increase in length of the pipe for a particular hole diameter (P6–P10), whereas it decreases with an increase in the pitch (P3 and P4). Similar trends were observed in the rest all of the cases. For ring spargers (Fig. 5) similar kind of observations was made. Non-uniformity increases with an increase in the hole diameter (R1–R3) and with an increase in the ring diameter for a fixed hole diameter (R4 and R5). Further, non-uniformity decreases with an increase in the pitch (R3 and R4). In all the above cases momentum and kinetic energy effects predominate over friction effects as holes near the closed ends discharge more than the holes near the entrance [1]. Friction and momentum effects work in opposite directions, the first tending to produce a pressure drop and the second a pressure rise [2]. The proper balance of two effects can result into less non-uniformity. When hole diameter increases (P1–P3) for a fixed pitch, the momentum effects become more domi-

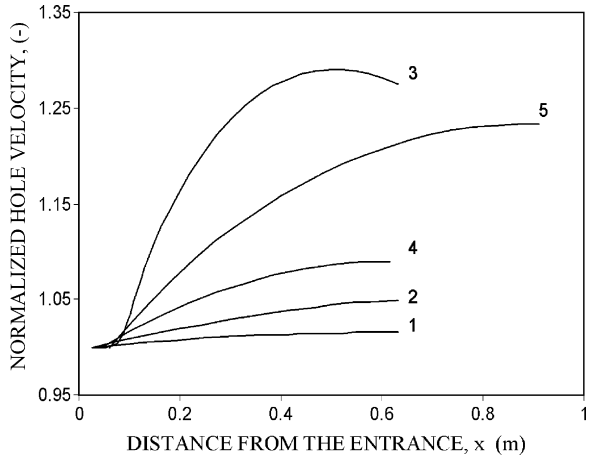

Fig. 5. Normalized hole velocity profile for ring sparger: (1) R1 (V_{in} = 28.71 m/s); (2) R2 (V_{in} = 29.06 m/s); (3) R3 (V_{in} = 26.65 m/s); (4) R4 (V_{in} = 23.09 m/s); (5) R5 (V_{in} = 25.5 m/s).

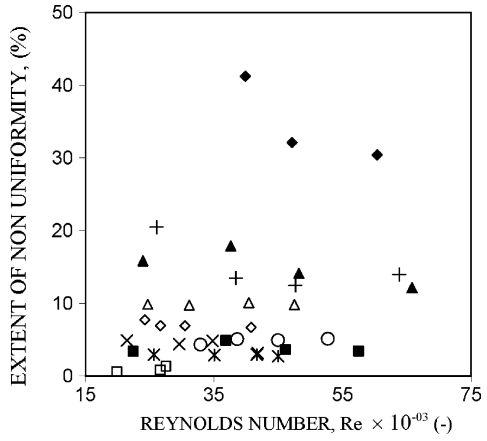

Fig. 6. Extent of non-uniformity for pipe spargers: (◊) P1; (□) P2; (△) P3; (×) P4; (*) P5; (◯) P6; (+) P7; (■) P8; (♦) P9; (▲) P10.

nant than the friction effects, hence non-uniformity increases. In the case of P3 (V_{in} = 28.4 m/s), the absolute value of rise in pressure from entrance to dead end (361 Pa) is much greater than (139 Pa) that in the case of P1 (V_{in} = 24.38 m/s). Therefore, more dominant effect of momentum in the case of P3 results into more non-uniformity. Increase of non-uniformity with increase in length for fixed pitch (P6–P10) can also be explained similarly. The absolute value of pressure rise from entrance to dead end for the case of P10 (V_{in} = 28.82 m/s) is 230 Pa, whereas for the case of P6 (V_{in} = 26.89 m/s) the value is 149 Pa. With an increase in the pitch for a fixed hole diameter (P3–P4), the friction between two consecutive holes increases. As a result friction effects become more prominent for pipe with higher pitch than with lower pitch, resulting into a less non-uniformity. This can also be brought out clearly from the absolute value of pressure rise from entrance to dead end. In the case of P4 (V_{in} = 24.99 m/s) the value of pressure rise is 292 Pa whereas for P3 (V_{in} = 28.4 m/s) the value is 361 Pa, which shows more prominent effects of friction in case of P4. The observations in the case of ring spargers can also be explained in the similar manner. Therefore, the hole diameter and pitch appear to be the most crucial parameters for a given length as far as uniformity is concerned. A judicious choice of both will ensure the proper balance between momentum effects and friction effects thus giving less non-uniformity.

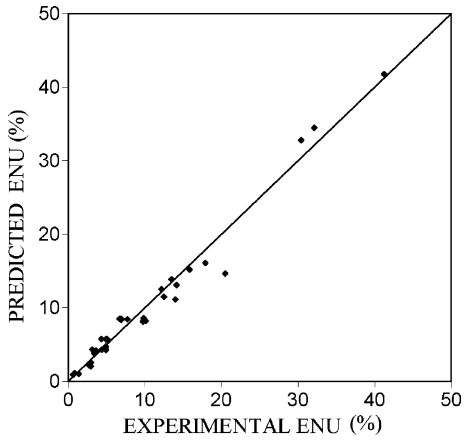

Fig. 7. Parity plot of extent of non-uniformity.

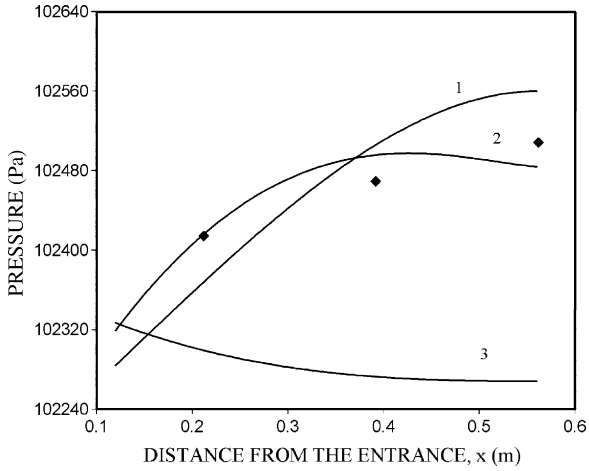

Fig. 8. Pressure profile from theoretical models for P1 (V_{in} = 24.38 m/s) ((♦) experimental value): (1) Acrivos et al. [2]; (2) Wang et al. [6]; (3) Cooper [3].

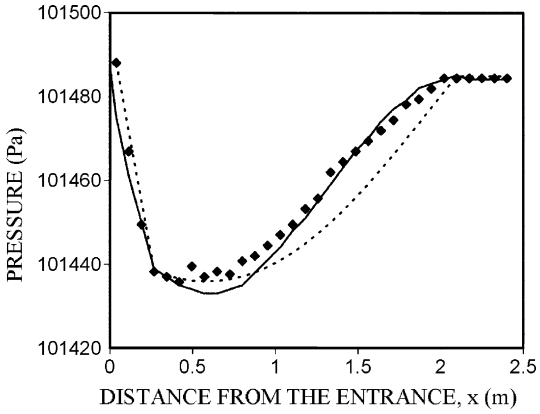

Fig. 9. Pressure profile for the geometry of Acrivos et al. [2] ((♦) experimental value): (—) CFD; (– – –) theoretical model [2].

At this point it is really interesting to find out how 'extent of non-uniformity' (ENU) varies with different geometrical and flow parameters for pipe spargers. Acrivos et al. [2] had defined

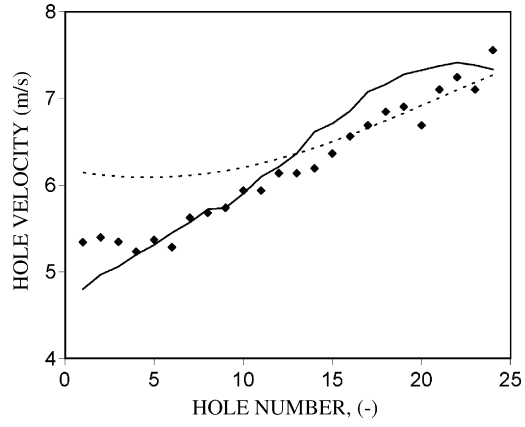

Fig. 10. Velocity through side hole for the geometry of Acrivos et al. [2] ((♦) experimental value): (—) CFD; (– – –) theoretical model.

ENU on the basis of first hole and last hole velocity as

$$\text{ENU} = \frac{\text{last hole velocity} - \text{first hole velocity}}{\text{first hole velocity}} \times 100 \qquad (44)$$

Fig. 6 shows the variation ENU with Reynolds number for all the pipe spargers. ENU is largest for P9 owing to the combination of large hole size (5 mm), small pitch ($4d_o$) and large length, whereas P2 shows smallest ENU due to its small hole size (2 mm), large pitch ($8d_o$) and short length. With this large number of experimental data, it was thought desirable to correlate ENU with different geometrical and flow parameter, which can be used as useful tool to get an idea of ENU for pipe spargers. Following are the results with a correlation coefficient of 0.91. The parity plot is shown in Fig. 7:

$$\text{ENU}=208.93 Re^{-0.20} Eu^{-0.64} \left(\frac{\Delta x}{d_o}\right)^{0.27} \text{FA}^{0.341} \left(\frac{\Delta x}{L_e}\right)^{-0.21} \qquad (45)$$

5.2. Analysis of analytical model

For efficient design of sparger either one has to perform large number of physical experiments with every possible combina-

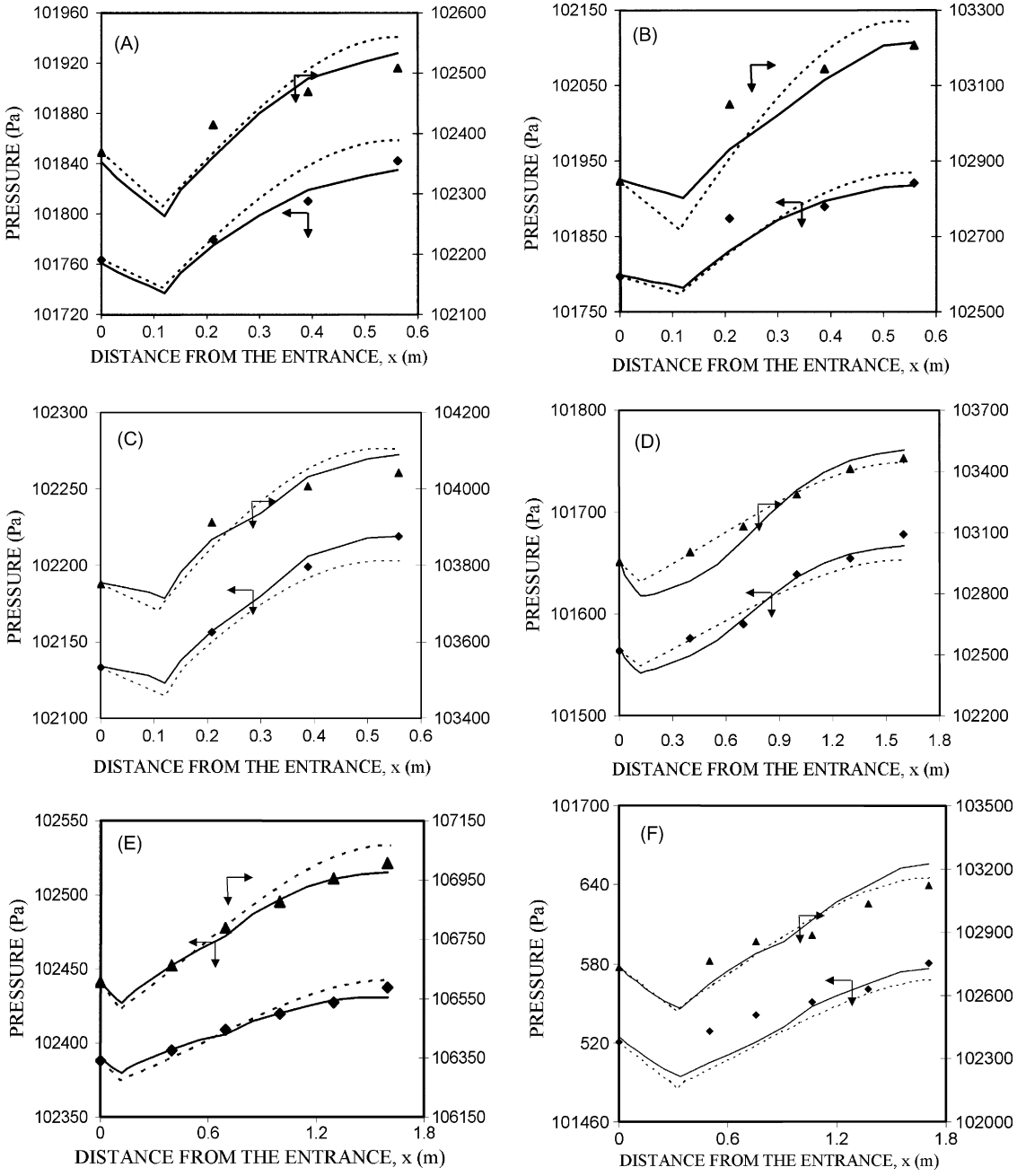

Fig. 11. Comparison of CFD and theoretical pressure profile with experimental value for pipe spargers. (A) P1: (♦) V_{in} = 14.5 m/s and (▲) V_{in} = 24.38 m/s; (B) P3: (♦) V_{in} = 14.76 m/s and (▲) V_{in} = 28.4 m/s; (C) P4: (♦) V_{in} = 12.84 m/s and (▲) V_{in} = 24.99 m/s; (D) P7: (♦) V_{in} = 15.60 m/s and (▲) V_{in} = 38.16 m/s; (E) P8: (♦) V_{in} = 13.40 m/s and (▲) V_{in} = 28.4 m/s; (F) P10: (♦) V_{in} = 14.33 m/s and (▲) V_{in} = 39.34 m/s ((—) CFD; (– – –) theoretical model [2]).

tion of hole diameter, pitch, and other geometrical parameters or otherwise a reliable analytical model is needed which describes flow inside the sparger quite well. There are three analytical models [2,3,6] available in the literature, which describes change in pressure and velocity along the length of the straight pipe sparger. The model proposed by Greskovich and O'Bara [4] gives only the total pressure change from entrance to dead end, and thus of little use as far as design of sparger is concerned. Acrivos et al. [2] had presented one of the most comprehensive analytical model, which takes into account both pressure rise phenomena within the sparger and flow variation through holes. The phenomena of pressure rise cannot be captured by a model proposed by Cooper [3] as it only considers Fanning's equation for describing flow inside sparger, whereas Wang et al. [6] considered the variation of k' along the length. Both Cooper [3] and Wang et al. [6] assumed uniform flow through holes and simplified the model. The assumption of uniformity through holes is justified in the case of Cooper [3] as he allowed the pitch to vary from entrance to dead end, but no such justification can be given for Wang et al. [6]. Fig. 8 shows a comparison among the three theoretical models for the straight pipe sparger P1 ($V_{in} = 24.38$ m/s). It can be clearly seen that the model by Cooper [3] cannot predict the pressure rise whereas the models by Acrivos et al. [2] and Wang et al. [6] can predict the pressure

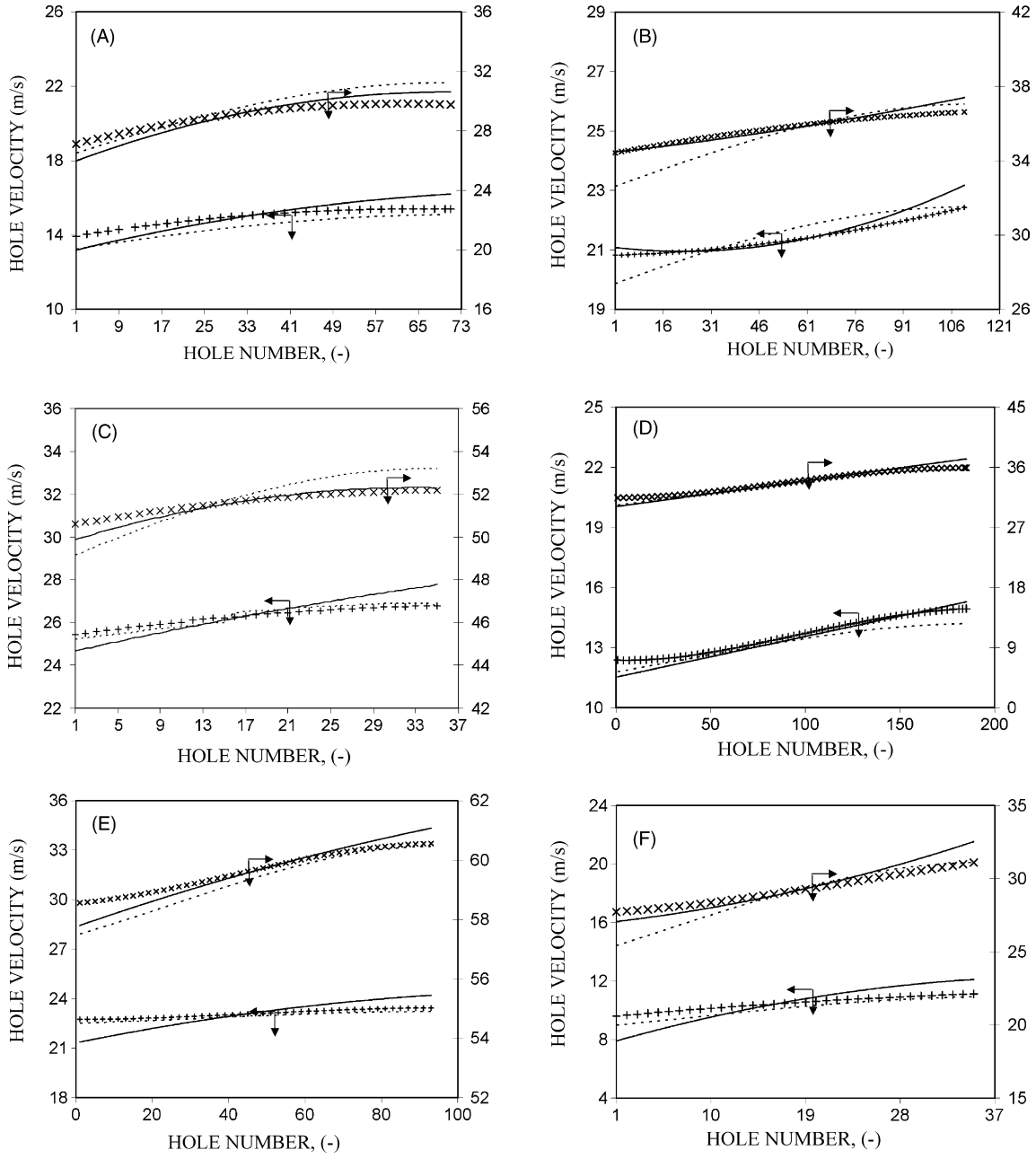

Fig. 12. Comparison of CFD and theoretical hole velocity with value calculated from pressure profile for pipe spargers. (A) P1: (+) $V_{in} = 14.5$ m/s and (×) $V_{in} = 24.38$ m/s; (B) P3: (+) $V_{in} = 14.76$ m/s and (×) $V_{in} = 28.4$ m/s; (C) P4: (+) $V_{in} = 12.84$ m/s and (×) $V_{in} = 24.99$ m/s; (D) P7: (+) $V_{in} = 15.60$ m/s and (×) $V_{in} = 38.16$ m/s; (E) P8: (+) $V_{in} = 13.40$ m/s and (×) $V_{in} = 28.4$ m/s; (F) P10: (+) $V_{in} = 14.33$ m/s and (×) $V_{in} = 39.34$ m/s ((—) CFD; (– – –) theoretical model [2]).

Table 3
Variation of k' and C in pipe spargers

Sparger no.	Inlet velocity (m/s)	Model of Acrivos et al. together with experimental data		Variation of k' and C across different hole from CFD												
		k'	C													
				Hole no.	1	3	5	20	35	50	65	80	90	100	105	110
P1	14.76	0.69	0.74	k'	0.53	0.53	0.54	0.57	0.58	0.70	0.72	0.75	0.73	0.75	0.76	0.77
				C	0.76	0.77	0.75	0.78	0.78	0.77	0.76	0.75	0.75	0.77	0.77	0.77
				Hole no.	1	3	5	15	25	35	40	50	60	67	69	71
P3	28.4	0.88	0.52	k'	0.45	0.41	0.46	0.50	0.47	0.47	0.52	0.59	0.87	0.85	0.87	0.88
				C	0.53	0.53	0.54	0.54	0.55	0.55	0.56	0.56	0.54	0.53	0.53	0.53
				Hole no.	1	2	3	4	10	13	15	20	25	30	34	35
P4	12.84	0.56	0.69	k'	0.48	0.47	0.49	0.50	0.61	0.63	0.65	0.66	0.66	0.67	0.66	0.66
				C	0.67	0.67	0.68	0.68	0.68	0.68	0.68	0.69	0.70	0.70	0.69	0.70
				Hole no.	1	7	20	45	60	75	90	105	125	155	180	185
P7	38.16	0.61	0.59	k'	0.43	0.45	0.44	0.45	0.48	0.50	0.52	0.58	0.60	0.67	0.72	0.74
				C	0.58	0.58	0.58	0.59	0.60	0.60	0.59	0.58	0.59	0.60	0.61	0.61
				Hole no.	1	3	5	15	26	46	55	68	75	89	91	93
P8	34.37	0.55	0.64	k'	0.43	0.44	0.47	0.45	0.47	0.47	0.46	0.50	0.52	0.58	0.64	0.68
				C	0.63	0.62	0.62	0.63	0.62	0.61	0.63	0.64	0.62	0.62	0.61	0.62
				Hole no.	1	2	3	4	10	13	15	20	25	30	34	35
P10	14.33	0.45	0.55	k'	0.48	0.49	0.49	0.51	0.52	0.48	0.49	0.49	0.50	0.51	0.49	0.50
				C	0.57	0.56	0.58	0.58	0.57	0.57	0.58	0.58	0.59	0.58	0.57	0.56

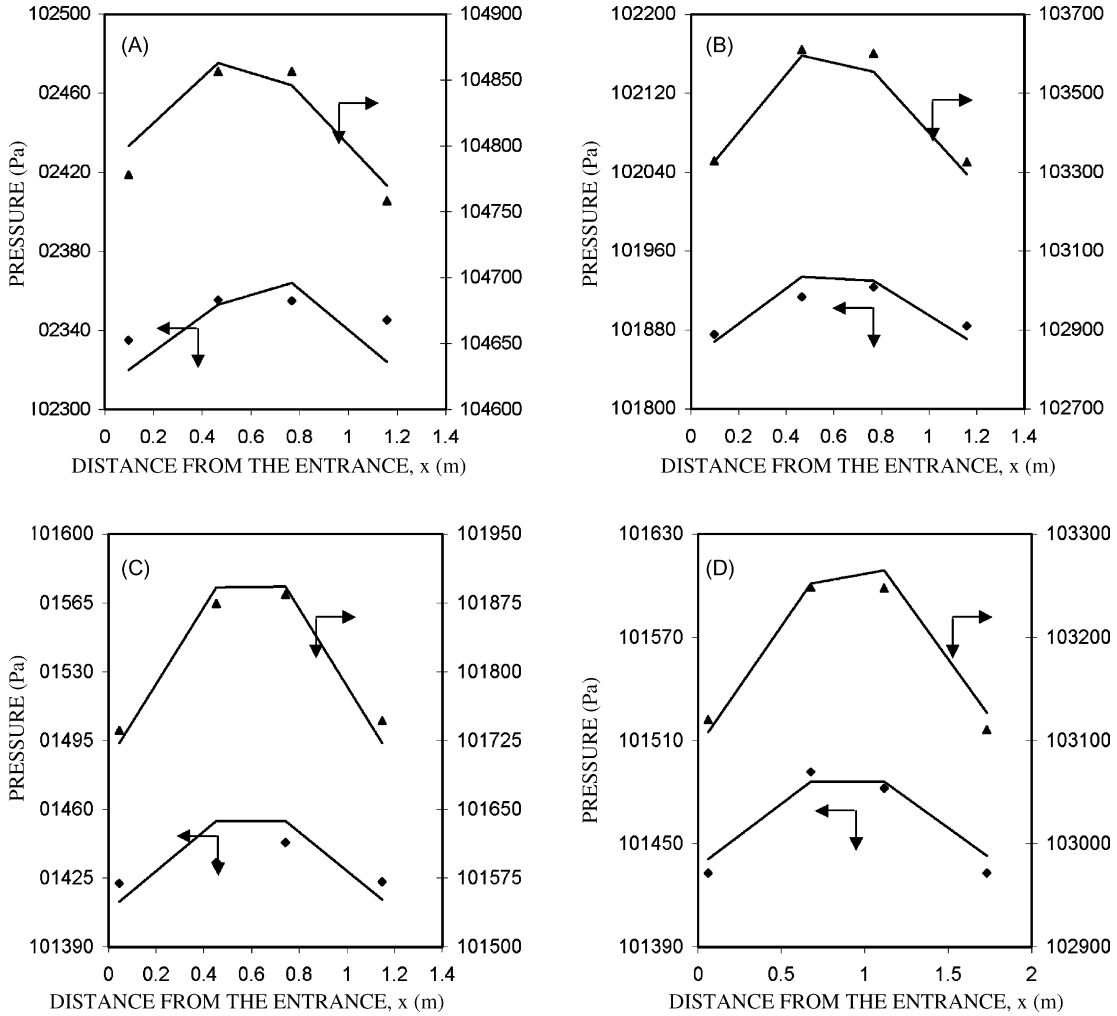

Fig. 13. Comparison of CFD and experimental pressure profile for ring sparger for two different velocities. (A) R1: (♦) V_{in} = 13.92 m/s and (▲) V_{in} = 28.71 m/s; (B) R2: (♦) V_{in} = 29.06 m/s and (▲) V_{in} = 58.5 m/s; (C) R4: (♦) V_{in} = 23.09 m/s and (▲) V_{in} = 52 m/s; (D) R5: (♦) V_{in} = 25.50 m/s and (▲) V_{in} = 96.56 m/s.

rise. The model of Acrivos et al. [2] over predicts pressure at the dead end due to the use of constant value of k'(experimental value of 0.80). Wang et al. [6] tried to de-bottleneck this problem incorporating varying k' along the length, but the assumption of uniform distribution limits the use of this model.

From the foregoing discussion it can be clearly seen that, the model proposed by Acrivos et al. [2] is the only theoretical model available which incorporates possibly all the features such as (i) pressure drop due to friction, (ii) pressure recovery because of the reduction in momentum and (iii) the non-uniformity of the sparger. However, this model needs a large experimental base which gives values of k' and C which are needed for all the estimations. Further, validity of this model for complex geometry, like ring sparger, had not been checked. All these limitations however can be mitigated by the use of CFD, which without the explicit knowledge of $k'$and C can estimate the pressure profile and flow distribution through hole for both pipe and ring sparger.

5.3. CFD versus Acrivos model

Along with the pressure measurements, Acrivos et al. [2] had also measured the hole velocity directly with pitot tube. Therefore, for the validation of CFD model, particularly for hole velocity, the data reported by Acrivos et al. [2] was simulated. The same data was also compared with their theoretical model. The results for pressure profile and the hole velocity are given in Figs. 9 and 10, respectively. It can be seen that the CFD gives a relatively favorable prediction over the earlier model for both pressure profile and hole velocity. Although the Acrivos model predicts pressure profile almost accurately, but it shows some deviation while predicting the hole velocity for the starting holes. Further, it may be pointed out that values of k' and C in the Acrivos model have been estimated from the experimental measurements of pressure profile and the hole velocities and hence the good agreement is in order.

With this favorable predictions of both hole velocity and pressure profile, CFD simulations for all the pipe and ring sparger were carried out. Simultaneously, the simulations with the model of Acrivos et al. [2] for all the pipes were performed. The pressure profile along the length of the pipe and velocity through the holes, for six straight pipe spargers (P1, P3, P4, P7, P8 and P10) with two different velocities are given in Figs. 11 and 12, respectively. It can be seen from Fig. 11 that, the CFD and the Acrivos model gives comparable predictions. For few cases (P1, P3 and P8) Acrivos model overpredicts the pressure values. Fig. 12 shows the values of absolute velocity through the holes. It can be seen that, for most of the cases, CFD predicts the absolute velocity quite well. The variation of k' and C along the length

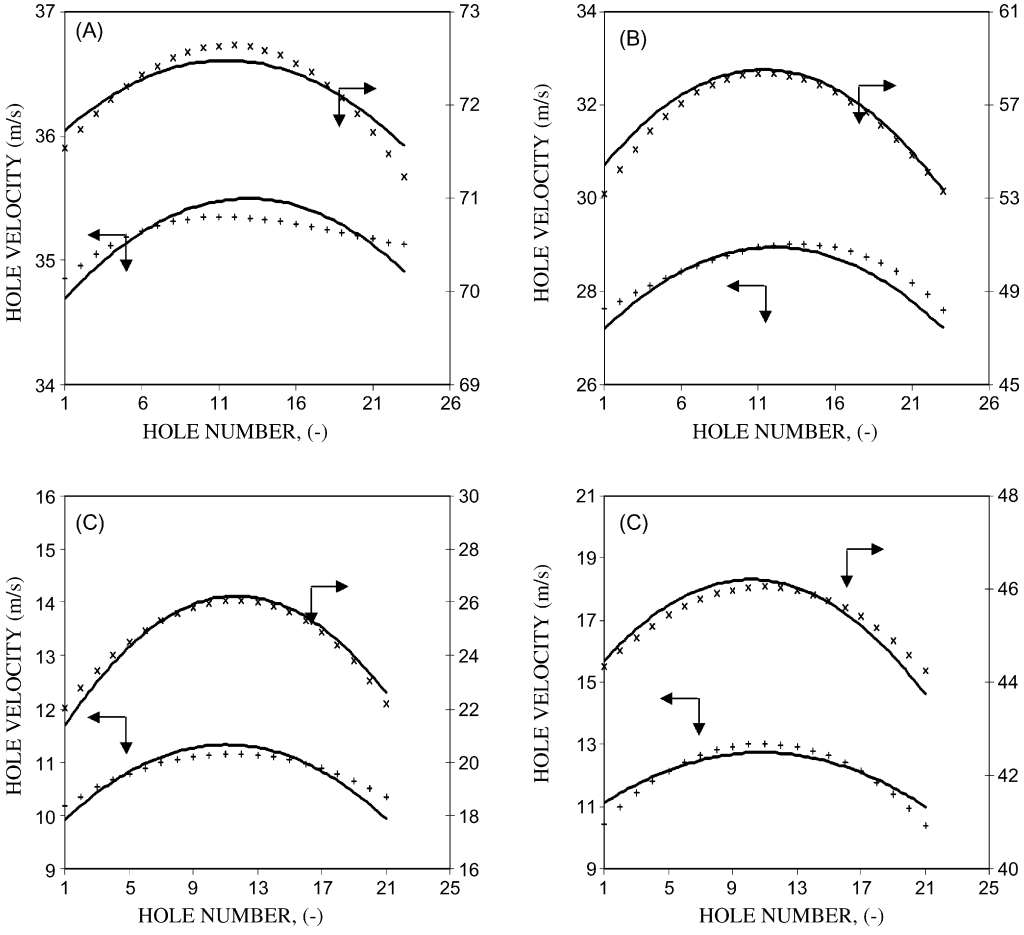

Fig. 14. Comparison of CFD and theoretical hole velocity with value calculated from pressure profile for ring spargers. (A) R1: (+) V_{in} = 13.92 m/s and (×) V_{in} = 28.71 m/s; (B) R2: (+) V_{in} = 29.06 m/s and (×) V_{in} = 58.5 m/s; (C) R4: (+) V_{in} = 23.09 m/s and (×) V_{in} = 52 m/s; (D) R5: (+) V_{in} = 25.50 m/s and (×) V_{in} = 96.56 m/s.

of pipe for P1, P3, P4, P7, P8 and P10 was estimated from CFD and the values for one case are given in Table 3. It can be seen that, k' increases along the length, which is in accordance with the assumption of Wang et al. [6], but the variation of C is very negligible. For a fixed pitch (P1 and P3) the variation of k' is larger for larger hole size, and for a fixed hole size (P3 and P4) variation of k' is smaller for larger pitch. These observations in turn explain the reasons for large non-uniformity for the cases of larger holes and smaller pitch.

The results of CFD simulation of pressure profile within the ring and velocity through the holes, for four rings (R1, R2, R4 and R5) are presented in Figs. 13 and 14. The predictions are well in agreement with the experimental values.

6. Conclusions

Experiments have been performed for the measurements of the pressure profile and hole velocities for the case of straight pipe as well as ring spargers. A wide range of hole diameter, pitch, pipe length and ring diameter have been covered. It was found that the non-uniformity increases with an increase in the free area and the length of the pipe sparger.

Correlations for k' and C for pipe sparger were developed from the experimental data. Further, the experimental data was used to quantify the extent of non-uniformity, and a correlation for the extent of non-uniformity was developed.

A critical analysis of available theoretical models was done, and it was found that the model proposed by Acrivos et al. [2] is most comprehensive. This model is capable of predicting pressure and flow distribution but only with prior information of k' and C which has to be obtained experimentally for a given sparger.

A CFD model has been used to simulate the pressure distribution and velocity profile for straight pipe sparger, and it shows favorable agreement for all the cases. Moreover, the CFD simulations do not need the value of k' and C as input.

A CFD model has been successfully used to predict the pressure distribution and the flow profile in ring sparger, for which no theoretical model is available in the published literature.

For the case of simple pipe sparger, the analytical model can be used. However, variations in the design (outside the range for which the values of k' and C have been reported) is beyond the scope of analytical models. For such cases the present work has shown the applicability of CFD models.

References

[1] V.E. Senecal, Fluid distribution in process equipment, Ind. Eng. Chem. 49 (6) (1957) 993–997.
[2] A. Acrivos, B.D. Babcock, R.L. Pigford, Flow distributions in manifolds, Chem. Eng. Sci. 10 (1959) 112–124.
[3] H.W. Cooper, Area allocation for distributor pipes, Chem. Eng. 10 (1963) 148–152.
[4] E.J. Greskovich, J.T. O'Bara, Perforated-pipe distributors, Ind. Eng. Chem. Proc. Des. Dev. 7 (4) (1968) 593–595.
[5] K.S. Knaebel, Simplified sparger design, Chem. Eng. 3 (1981) 116–118.
[6] J.G. Wang, Z. Gao, G. Gan, D. Wu, Analytical solution of flow coefficients for uniformly distributed porous channel, Chem. Eng. J. 84 (2001) 1–6.